Mechanism and Machine Theory 163 (2021) 104372

Contents lists available at ScienceDirect

Mechanism and Machine Theory

journal homepage: www.elsevier.com/locate/mechmachtheory

Human-robot cooperative control system based on serial elastic actuator bowden cable drive in ExoArm 7-DOF upper extremity exoskeleton

Paweł Herbin*, Mirosław Pajor

Faculty of Mechanical Engineering and Mechatronics, West Pomeranian University of Technology, Szczecin, Piastów av. 19, 70-310 Szczecin, Poland

ARTICLE INFO

Article history:
Received 4 January 2021
Revised 13 April 2021
Accepted 13 April 2021

Keywords:
Exoskeleton design
Exoskeleton
Bowden cable
Wearable robots
Serial elastic actuator
SEA

ABSTRACT

The exoskeleton of the upper limb is an external parallel kinematic chain to the human arm. The device is designed to apply a specific torque of interaction to the human body resulting from bilateral teleoperation or rehabilitation. Its task is to work comfortably with the human arm. This paper presents the structure of the developed device and the control system of its joints. The construction of the joints' drive system was performed based on the Bowden cable transmission. Based on the Bowden cable flexibility, it is possible to control the generated drive torque following the serial elastic actuator concept. The article presents joint control methods minimizing the influence of friction in the closed-loop Bowden cable conduit system. We also present the methods of estimating the torque of interaction with the operator based on the ExoArm 7-DOF exoskeleton dynamics model.

1. Introduction

Wearable robots such as exoskeletons are particularly useful in rehabilitating human beings, increasing human muscle strength, and controlling machines. In recent years many teams have developed the structure of these devices and their control systems [1–21]. Regardless of its application, the human-robot interface must be adapted to a quick and effective reading of the operator's intentions. This is the key to the smooth interaction between the wearable robot and the user. Calculating the operator's intention requires measuring the torque of the interaction force acting on a human body. The torque acquisition can be implemented directly using force sensors placed between the operator's body and the wearable robot [22]. The type of the applied method of measuring the torque of the interaction force depends on the way the robot is driven. Direct drives enable the implementation of drive torque estimation based on the motor current [23,24]. In the closed-loop cable conduit system, it is possible to integrate the measuring systems with the drive system component [25]. Draw gears are used more and more frequently to reduce the weight of the machine's moving parts, thus improving the wearable robot's dynamic properties. These enable the removal of heavy drive system components, which are motors, to a stationary stand. Using the cable transmission system results in a significant reduction in the machine's weight and a significant reduction in the torques that have to be applied by the robot actuators. The closed-loop cable conduit system is

* Corresponding author.
E-mail address: pawel.herbin@zut.edu.pl (P. Herbin).

https://doi.org/10.1016/j.mechmachtheory.2021.104372

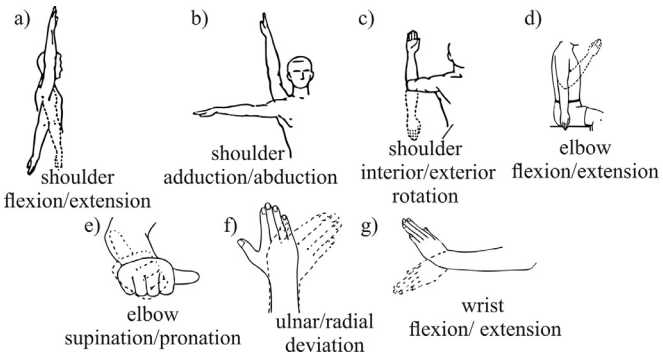

Fig. 1. Upper extremity movements: a) shoulder flexion/extension, b) shoulder adduction/abduction, c) shoulder interior/exterior rotation, d) elbow flexion/extension, e) elbow supination/pronation, f) wrist ulnar/radial deviation, g) wrist flexion/extension.

Table 1
The most advanced exoskeleton structures.

No.	Name	Research team	Number of joints	Type/location of drive units
1	IntelliArm	Rehabilitation Institute of Chicago (Park, Yupeng Ren, and Li-Qun Zhang 2008)	7 active 2 passive	actuators placed directly at the joints
2	SUEFUL-7	Saga University Japan (Gopura, Kiguchi, and Li 2009)	7 active	DC motors directly drive 4 joints, 3 joints are driven by cable transmision
3	EXO-UL8	Bionics Lab, University of California Los Angeles (Y. Shen et al. 2018)	8 active	torque actuators located directly at the device structure

built based on two flexible steel cables routed in a flexible steel sheath. When one of the tendons is pulled by the actuator, it slides in the hollow flexible sheath. Owing to the cables routed in the sheath, there is no elaborate pulleys system in the moving structure [26,27]. It is necessary to note that the tendons' sliding movement in the sheath system generates significant frictional forces, which result in many disorderly phenomena, such as backlash and hysteresis in the closed-loop cable conduit system. Furthermore, those phenomena are a significant challenge to the precise control of the joint position precise control and the actuator torque. A feed-forward system has been designed to compensate for the most undesirable influence of frictional effects (in the tension transmission system). The efficiency of the implemented friction compensation was tested experimentally. With the use of tendon systems, the change of the cable configuration in space significantly affects the friction parameters and the initial tension of the cables. A spring pre-tensioner was placed in the transmission structure to reduce this effect. Its function is to compensate for backlash in the closed-loop cable conduit system.

In this paper, we described the mechanism of an exoskeleton with seven degrees of freedom. In the proposed solution, a spring pre-tensioner was placed in the drive system to initially stretch the cable and increase the precision of control of the torque generated on the exoskeleton joints. The functionality of this solution was verified experimentally. This article describes the control methods of ExoArm 7-DOF joints, which can be used in bilateral teleoperation. Section 2 of this article describes the system's kinematic structure concerning the movements of the human upper extremity. Section 3 introduces the structure and characteristics of the drive system. The methods of controlling the joints with a feed-forward from friction are presented in Section 4. The results of the experiments on the operation of control systems are presented in Section 5. The last part of this article, summarizes the results and present the guidelines for further research.

1.1. Kinematic structure of an upper limb exoskeleton

The kinematic structure of wearable robots must be adapted to the human limb. For this purpose, the development of the kinematic structure must be preceded by an analysis of the extremity movement anatomy mechanism and the range of its movement for the future operator. Based on the analysis of the mobility of the upper limb joints, the motions that can be implemented by the upper limb are listed below (see Fig. 1): shoulder flexion/extension, shoulder adduction/abduction, shoulder interior/exterior rotation, elbow flexion/extension, elbow supination/pronation, wrist ulnar/radial deviation and wrist flexion/extension. Researchers have proposed many complex kinematic structures of exoskeletons to implement the upper limb full mobility. The most advanced structures of exoskeletons include IntelliArm [28], SUEFUL-7 [18], and EXO-UL8 [29]. Their properties are presented in Table 1. The exoskeletons described in this table represent structured with active joints. The mentioned devices are very advanced exoskeleton structures reproducing the full kinematics of the upper structure, however, they use different numbers of joints. These solutions include wearable robots with direct drives and actuators with transmissions. In our proposed device, all drives are realized by a cable transmission and SEA drive. In this way we achieved a significant reduction the mass of moving components of our exoskeleton.

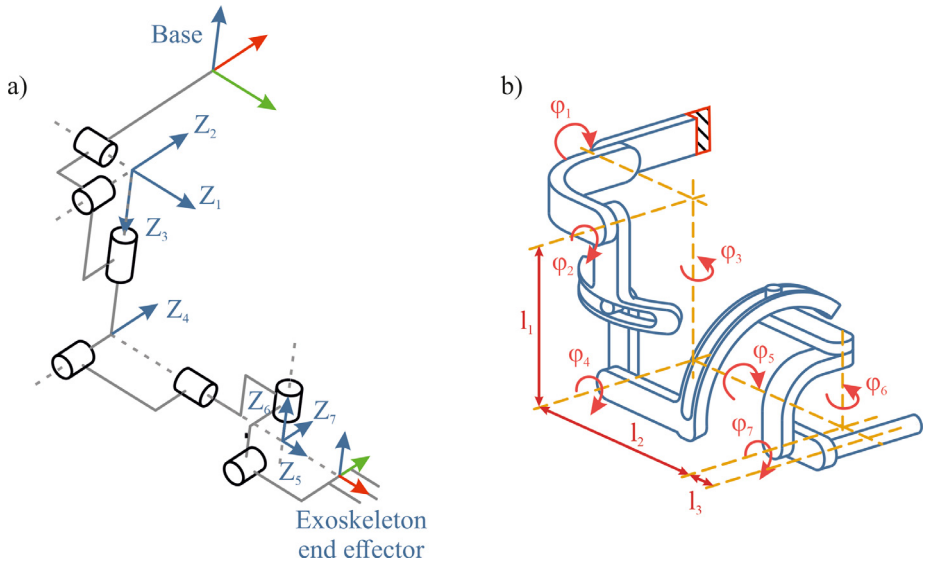

Fig. 2. Exoskeleton ExoArm 7-DOF a) kinematic structure b) scheme of device construction.

Table 2a
D-H parameters of ExoArm 7-DOF.

i	Link	α_i	a_i	d_i	Θ_i
0	Base	0°	0	0	0
1	Shoulder	–90°	0	0	$\beta_1 + 90°$
2	Shoulder	+90°	0	0	$\beta_2 + 90°$
3	Shoulder	0°	l_1	0	$\beta_3 + 90°$
4	Elbow	+90°	0	0	$\beta_4 + 90°$
5	Elbow	+90°	0	l_2	$\beta_5 + 90°$
6	Wrist	+90°	0	0	$\beta_6 + 90°$
7	Wrist	+90°	l_3	0	β_7

The solution concerning the wearable robot that we propose is based on seven rotational joints. Their kinematic structure is developed explicitly in order to keep the workspace of the human upper extremity intact. The kinematic structure of this device consists of three groups of joints that result from the natural division of arm movements. The first group is responsible for the movements of the shoulder joint, the next one for the elbow joint and forearm movements, and the last one for the movements of the wrist. The kinematic structure of our exoskeleton construction called ExoArm 7-DOF is shown in Fig. 2a. Concerning the presented kinematic structure, Fig. 2b shows a simplified drawing of the device with a representation of the distance between the rotary axis, which should be adjusted to the operator and the configuration angles of the controllable joint. To effectively control the machine's motion, it was necessary to prepare a simple kinematics model of ExoArm 7-DOF and a dynamics model. Those models were used during the implementation of the device control system to achieve the movement of the system while controlling the torque generated on the machine's joints. The implemented models allowed to reduce the load on the operator.

The parameters of the kinematic model using Denavit-Hartenberg notation are shown in Table 2. Homogeneous transformation matrices have been defined based on the D-H parameters. The position of the handgrip against the global coordinate system is described by Equation 1.

$$ {}^{0}_{8}\mathrm{F} = \prod_{i=1}^{8} {}^{i-1}_{i}\mathrm{F} \tag{1} $$

Where ${}^{i-1}_{i}\mathrm{F}$ is the homogeneous transformation between i-1 and i coordinate system.

The location of each of the systems is based on anthropomorphic research. Distances l_1, l_2, and l_3 and the angle ranges of the joints are measured during the SFTR examination of the future exoskeleton operator. For specific lengths, the necessary parameters of the device's dynamics model are determined, i.e., the centre of gravity position, mass, and moments of inertia of the device's movable elements. The device's dynamics model was used in the device control algorithm in the torque control mode.

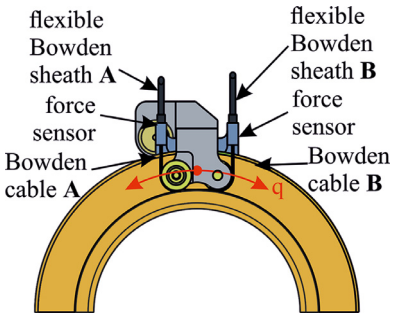

Fig. 3. Exoskeleton ExoArm 7-DOF rotary joint type I.

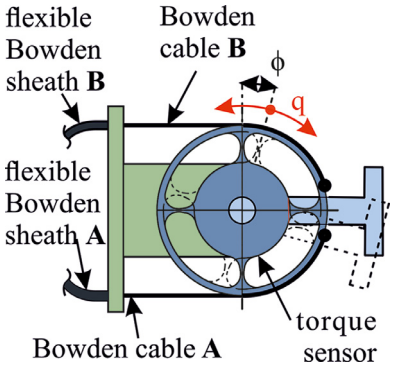

Fig. 4. Exoskeleton ExoArm 7-DOF rotary joint type II.

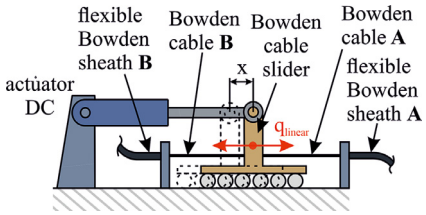

Fig. 5. Exoskeleton ExoArm 7-DOF actuator stand.

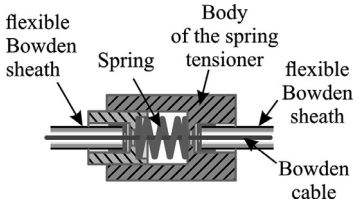

Fig. 6. Scheme of the spring pretension.

1.2. Closed-loop cable conduit system for the exoskeleton

We used Bowden cable drive systems to reduce the weight of the moveable parts of the ExoArm 7-DOF wearable robot, as shown in Figs. 3-5. The drive system consists of a fixed actuator base (see Fig. 5), exoskeleton rotary joints (see Fig. 3 and 4), and Bowden cables with spring pretension (see Fig. 6).

The applied transmission provides a constant ratio of force to drive torque. Regarding the relatively high flexibility of the cables, it is possible to achieve a Series Elastic Actuator (SEA) functionality of the drive. The cable transmission system is also equipped with a spring pretension, which increases the mechanism's flexibility, resulting in increased torque control precision (measured at the output of the cable transmission system). Increasing the flexibility of the transmission reduces the sensitivity of the control system to phase shifts. A DC actuator and a rod guide are attached to the fixed base of the drive stand. This cart moves on a ball bearing guide, depending on the actuator's movement direction, pulling the cable A

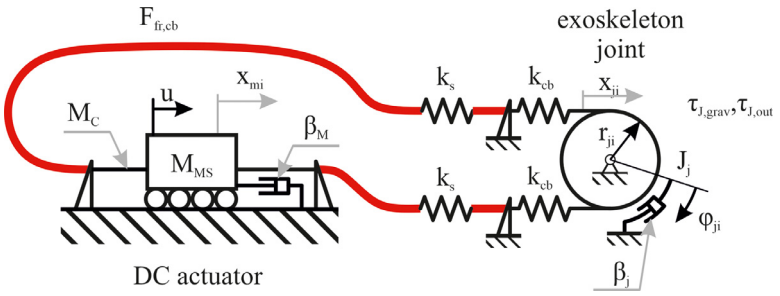

Fig. 7. Phenomenological model of a closed cable conduit system.

or B. The drive stand is connected to the ExoArm 7-DOF joint by a flexible Bowden cable sheath. The drive system of all joints is similar in design. The exoskeleton joints can be divided into two types:

- Type I – large diameter joints with a non-accessible rotation axle,
- Type II – relatively small diameter joints with an accessible rotation axis.

The type I joint is made of two strain-gauge beams and a cable guide in a full or half-ring (see Fig. 3). In this type of joint, the tension force values of all A and B cables are measured. The torque generated by the transmission is calculated from the difference of the tension force of two cables multiplied by the cable guide radius. The advantage of the first type of joint is the possibility to move the operator's extremity around. This type of joint is used in the third and fifth axes of the ExoArm 7-DOF exoskeleton.

The type II joint (see Fig. 4) consists of a cable pulley integrated with a strain gauge torque sensor [30]. This type of joint is used in the 1, 2, 4, 6, and 7 axes of the wearable robot. Torque is transmitted by A and B Bowden cables to a DC actuator mounted on a fixed base. In this case, the torque is measured directly with the torque sensor.

The control of the output torque using a cable transmission and a ball screw DC actuator is only possible based on the cables' flexibility. The drive torque generated by the electric motor is proportional to the current. However, in linear actuators, the gearbox excludes effective torque control by the current. In our solution, the closed cable conduit system is flexibility inserted between the ball screw DC actuator and the ExoArm 7-DOF joint. The phenomenological model of the transmission system is shown in Fig. 7. Based on the Hooke's law, the stiffness of the transmission cable for joints was calculated according to Equation 2.

$$k_{cb\ i} = \frac{EA}{l_i} \tag{2}$$

For the 2 mm diameter cables with a wire strand 1 × 19 structure, the metallic cross-sectional area is $A = 2.16\ \text{mm}^2$, and Young's modulus for such cables is $E = 140\ \text{kN/(mm}^2)$.

It is important to note that the Bowden cables only work when they are pulled. The force $F_{fr,cb} = \beta_{cb}\dot{x}_{mi}$ is the friction between the Bowden cable and the elastic sheath. The value of friction force in the cables is fluctuating about the Bowden cable sheath deflection, as described in more detail in [31–33]. The friction forces inside the ball screw gearbox, $F_{fr,m}$, are negligible, whereas the torque of force derived from gravity is significant, $\tau_{j,grav}$. Moreover, it has a considerable variation depending on the exoskeleton configuration.

$$(M_{MS} + M_C)\,\ddot{x_{mi}} + F_{fr,m} = u - F_{ms} \tag{2a}$$

$$F_{fr,m} = \beta_M \dot{x}_{mi} \tag{3}$$

$$\beta_j\,\dot{\varphi}_{ji} + J_j\,\ddot{\varphi}_{ji} = \tau_{j,out} + \tau_n \tag{4}$$

$$\tau_n = r_{ji}\frac{k_s \cdot k_{cb}}{k_s + k_{cb}}\left(x_{mi} - x_{ji}\right) \tag{5}$$

$$F_{ms} = \frac{k_s \cdot k_{cb}}{k_s + k_{cb}}\left(x_{mi} - x_{ji}\right) - F_{fr,cb} \tag{6}$$

Where:

u–control value;
F_{ms}–tension pull force of the Bowden cable;
φ_{ji}– angular position of the joint;

Table 2b
Parameters of the model of the 4th joint drive system.

Parameter	Parameter name	Value	Unit
M_{MS}	Transmission slider mass	$3.54*10^{-6}$	kg
M_C	Cable mass	$2.4*10^{-5}$	kg
J_j	Moment of inertia of moving parts	$6*10^5$	kg/m^2
β_M	Slide movement resistance	1.37	Ns/m
β_j	Join friction	5.1	Ns/m
β_{cb}	Bowden cable friction	7.21	Ns/m
k_s	Spring stiffness	*set value*	N/mm
k_{cb}	Bowden cable stiffness	$1.512 * 10^5$	N/m
r_{ji}	Cable wheel radius	$4*10^{-2}$	m

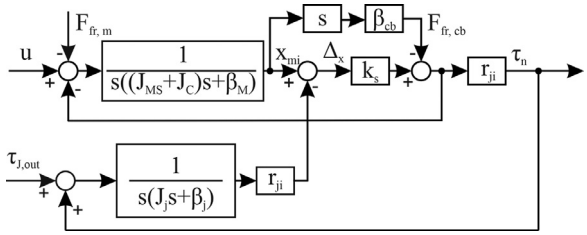

Fig. 8. Block diagram of the cable transmission system.

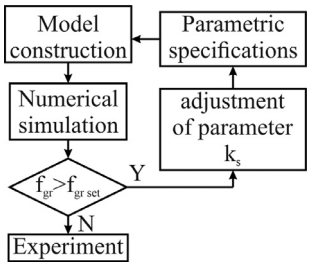

Fig. 9. The iterative algorithm of k_s value adjustment.

Table 3
Stiffness of additional springs in ExoArm-7DOF joint transmission chain.

Exoskeleton joint	1	2	3	4	5	6	7
$k_s(N/mm)$	13.2	13.2	8.4	8.8	6.2	4.5	4.1

$\tau_{j.out}$ – external load of the joint.

The rest of the transmission model parameters for the example joint (4) are listed in Table 2. Based on the equations, a block diagram shown in Fig. 8 was developed.

Exoskeleton joint drives are designed to precisely control the torque. Owing to the introduction of additional flexibility in the transmission path, it obtains the features of a SEA. A modification of the cable transmission flexibility allows for modifying the dynamic properties of the transmission system. The implementation of flexibility increases the precision of the torque control and increases the control system's stability margin. Adjusting the stiffness of the additional spring, k_s, is essential to increase the precision of torque control with the relevant limiting frequency at which the system can work efficiently. The limit frequency for human devices' control system should be higher than 10 Hz due to the human perception limits [34]. In this work, the minimum boundary frequency($f_{gr\ set}$) for the control system was set at 100 Hz. A frequency analysis was performed for each joint to select the k_s spring stiffness in the transmission chain of each joint. Adjustment of the compression spring stiffness was realized iteratively based on the algorithm in Fig. 9. Simultaneously, with the stiffness value adjustment in equations 2 – 6, the system's amplitude-frequency and phase-frequency characteristics were observed. The criterion for termination of the iteration is to achieve the resonance frequency (f_{gr}) at the limit frequency level. The determined stiffness values of spring k_s of joints, 1 – 7 of ExoArm-7DOF are shown in Table 3. The influence of a change in the cable transmission's stiffness on amplitude-frequency and phase-frequency characteristics is presented in Fig. 10. The introduction of additional flexibility (reduced stiffness) in a cable transmission results in a significant reduction in resonance amplitude and resonance frequency.

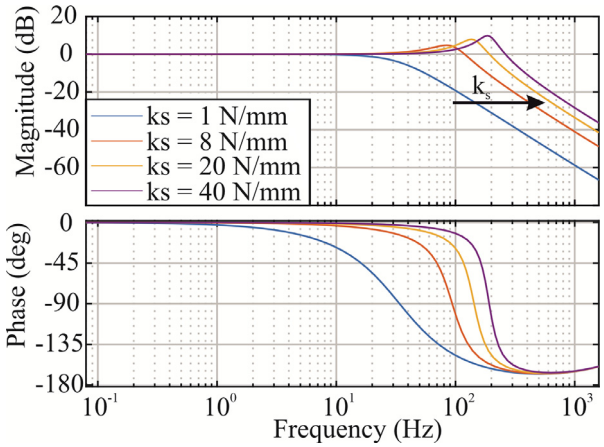

Fig. 10. The impact of ks spring parameters on magnitude-frequency and phase-frequency characteristics of ExoArm 7-DOF closed-loop cable conduit system.

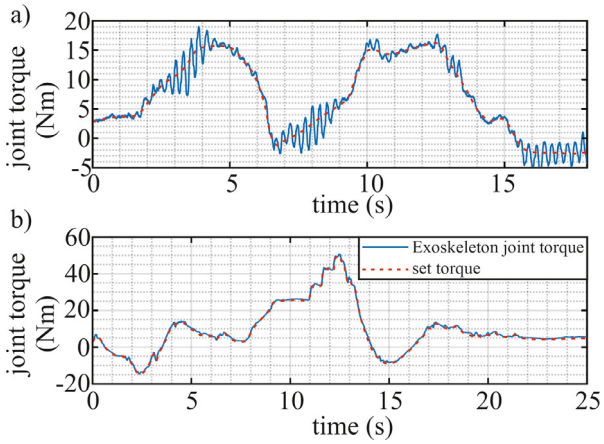

Fig. 11. Comparison of operation of the fourth joint control systems: a) without spring tensioner b) after installation of the additional flexibility.

A comparison of the torque control system's operation without the introduction of an additional spring and after its installation is shown in Fig. 10. The waveforms represent the torque values measured on the fourth joint. Insufficient flexibility of the transmission mechanism with the DC ball screw actuator results in an oscillation of the generated torque on the joints of the wearable robot (see Fig. 11a). After the implementation, an additional flexible component in the transmission chain, a significant improvement in the wearable robot's stability during the movement of the joints is obtained (see Fig. 11b). Furthermore, the torque oscillations generated during the joint movement during starting and stopping are significantly reduced.

1.3. Experimental stand

A prototype ExoArm 7-DOF exoskeleton was developed based on the kinematic model. In the device, we implemented a cable transmission system made using the Bowden cables. The device's construction is manufactured using 7075 aluminium alloy and Ti6Al4 V titanium alloy (manufactured in Selective laser melting technology). The upper extremity's exoskeleton is divided into individual moving components, and their joints are shown in Fig. 12. The developed device is operated by the National Instruments PXI (National Instruments, Austin, Texas, USA) controller equipped with LabView Real-Time software. Programmable H-bridges Pololu Simple High-Power Motor Controller 24v23 produced by Pololu (Pololu Corporation, Las Vegas, Nevada, USA) have been used to control DC linear actuators. The control signal for Pololu's bridges is analogue in the range 0~5 V. To measure the position of the joints, CUI AMT-203 V (CUI Inc., Tualatin, Oregon, USA) rotary pulse transducers with a resolution of 4096 pulses per revolution were used, resulting in an angular control resolution of 0.088°.

The torque sensors implemented in the ExoArm 7-DOF exoskeleton were designed and manufactured especially for this application and are described in more detail in [30]. For measuring the surface deformation of the designed sensors for steel components, we use strain gauges HBM 1-LY11–0.3/120 and 1.7225 (50HM) and 1-LY13–0.3/120 for components made of 7075 aluminium alloy (PA9). An amplifier ESAM Traveller CF (ESA Messtechnik GmbH, Mögglingen, Germany) was used

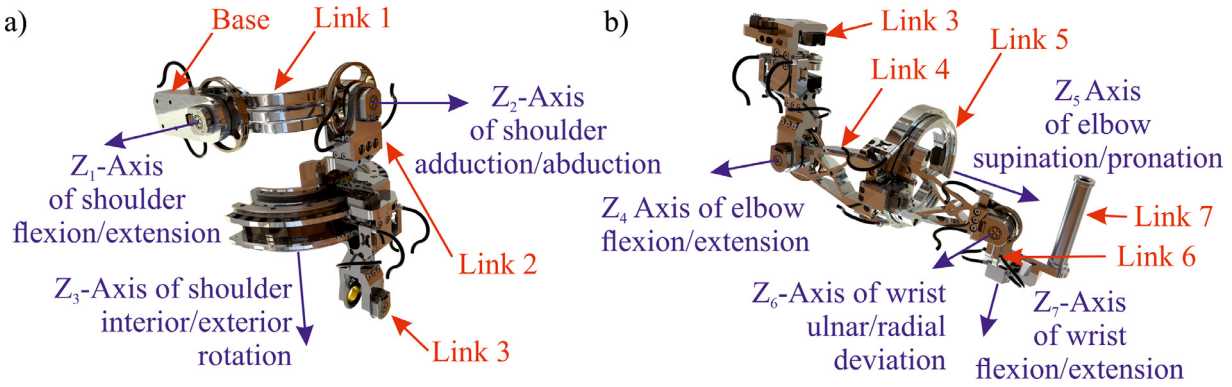

Fig. 12. a) 3-DOF shoulder joint b) 2-DOF elbow joint and 2-DOF wrist joint.

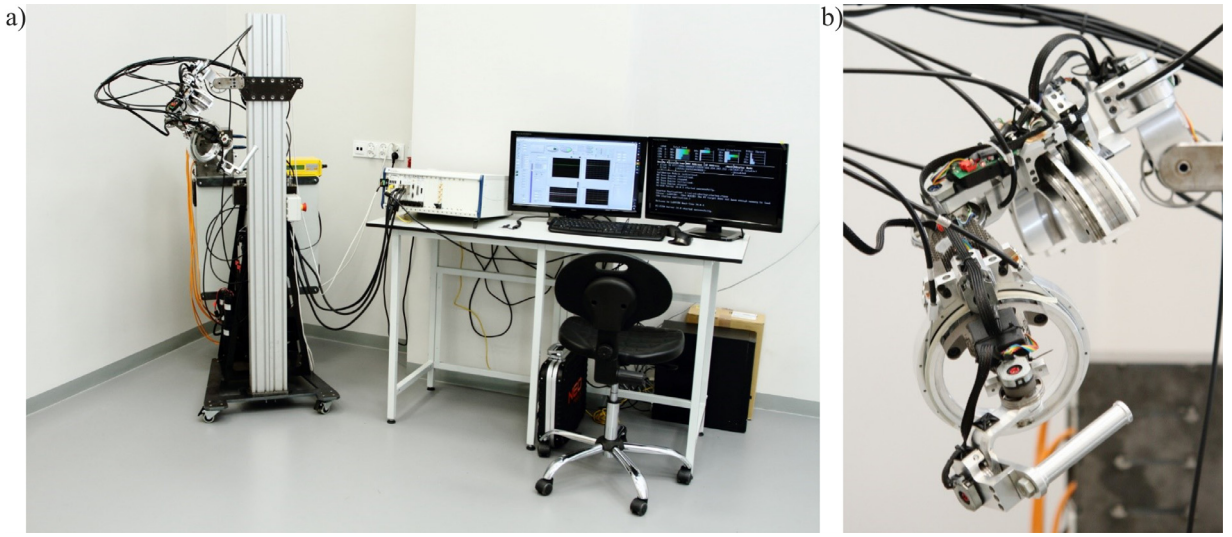

Fig. 13. Experimental stand of the upper extremity exoskeleton ExoArm 7-DOF a) ExoArm 7-DOF prototype with a control system b) ExoArm 7-DOF.

to perform strain gauge measurements. The complete and operationally ready equipment is presented in Fig. 13. Fig. 13a demonstrates a prototype with a control stand based on Ni PXI. Fig. 13b presents the ExoArm 7-DOF exoskeleton prototype connected to the tensioning system and drives via Bowden cables. During the tests, the prototype of the exoskeleton was located on a stationary fixture.

1.4. Control methodology

Controlling a device with such a complex kinematic structure is a very complicated process due to the mutually influencing motions of the joints on each other. Therefore, a model of dynamics of the object has been implemented in the control system. The drive system presented in the closed-loop cable conduit system for the exoskeleton section has force/torque sensors in its structure, which are applied to each joint. The disadvantage of this solution is that the sensor measures the combined effect of the device components movement, gravity forces, and the interaction torque with the device operator. To determine the interaction torque (τ_i) from the measured signal, it is necessary to subtract the value resulting from the object dynamics (τ_d) from the measured value (τ_m). τ_d is calculated using a dynamics model established by the Newton-Euler iterative method [35,36]. The model parameters were identified during the experimental study. Knowledge of the angular position (φ_f) of each joint as well as velocity (ω_f) and acceleration (ε_f) is necessary to calculate the torque applied to the rotary joint due to the movement of the components and the gravity force. This value is calculated from the angular position (φ_m) using the LS filter algorithm presented in [37]. The applied LS filter allows for filtering with a near-zero phase shift as well as the calculation of the derivatives (ω_f, ε_f) of the filtered signal. A diagram of the model used to calculate the interaction torque is shown in Fig. 14.

Control of the interaction torque in the exoskeleton's controlled axes is based on the model of the closed-loop cable conduit system described in this article. Consequently, the control system was based on the flexibility of the compression

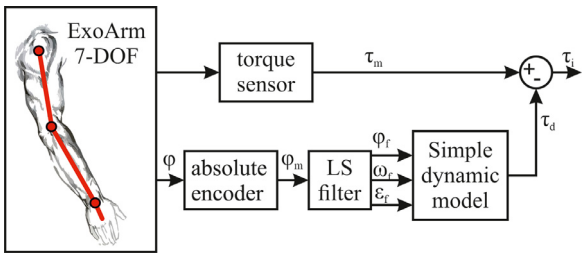

Fig. 14. Scheme of calculation of interaction torque (τ_i).

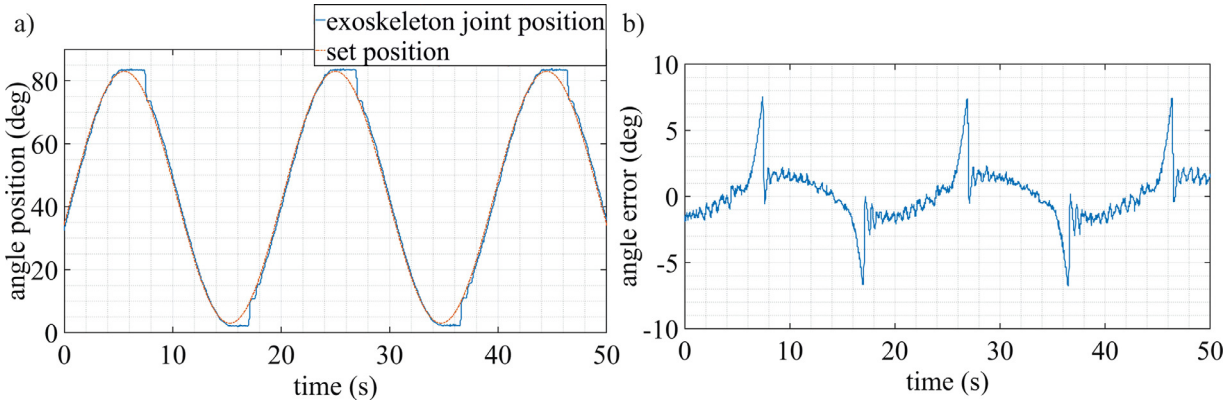

Fig. 15. Bowden cable friction phenomena during exoskeleton joint movement, a) angular position of the joint b) position error.

spring in the transmission path. It is possible to control the interaction torque in the exoskeleton joint using the actuator's position corresponding to it. The DC motor of a linear actuator used in the drive system is controlled by controlling its extension velocity. The application of the cable gear in the transmission path introduces significant non-linearities in the joint's operation. The impact of friction forces is mostly visible when the direction of movement of the joint is changing. The experimental test was performed for the joint position control system (see Fig. 15) without a spring pretension to show this phenomenon. A significant dead zone is observed when redirecting the movement of the joint. In order to minimize this effect, a friction compensation module was implemented in the control system. During testing a series of different friction compensation methods [38–40] in cable systems, the best results were obtained with the Stribeck effect compensator.

The Stribeck effect compensation has been applied in the final form of a control system for exoskeleton joints equipped with cable transmission. It provides a significantly faster start-up of the DC linear actuator motors when the joint changes its movement direction. As a result, the dead zone of the transmission path was significantly minimized. The risk of the insensitivity zone is also eliminated by applying the elastic elements in the compressed spring form in the cable transmission. The PID regulator structure was used with a feed-forward from the Stribeck compensation (see Fig. 16) to control the exoskeleton joints. The developed kinematic structure, mechanical structure, and the joint control system implement the task of forces feedback into the operator's arm. The Stribeck effect compensator (7) was used as a feedforward in the control system structure.

$$C_{strbieck}(s) = sign(u_{PID}(s))e^{\dot{x}(s)} \tag{7}$$

Where:

$C_{stribeck(s)}$ – feedforward compensation value;
$u_{PID}(s)$ – PID control value;
$\dot{x}(s)$ – actual joint velocity.

The DC actuators' connection with a flexible transmission allows for controlling the torque generated on the joint by controlling the movement of the DC actuator rod. The transmission flexibility provides the possibility of precise control of the torque. The presented control system basis is the torque measurement carried out by strain gauge sensors in the exoskeleton joints. Besides, an algorithm of software limit switches is used in the control system, which can be adjusted to the restrictions of the upper extremity movement for the future operator. They constitute additional protection apart from the mechanical protection of the joints.

The control algorithm presented in this article enables the implementation of two functionalities:

a) The implementation of the exoskeleton's movement is consistent with the movement of the human upper extremity with the device's unloading.

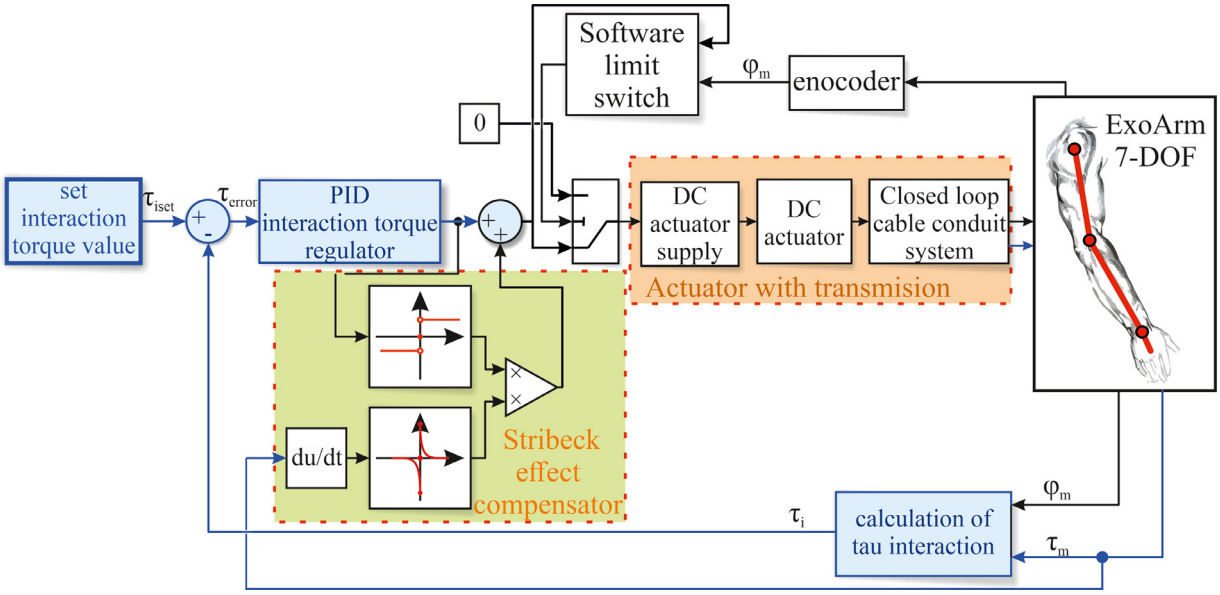

Fig. 16. Scheme of the interaction torque (τ_i) control system with the Stribeck effect compensator and positional software limiters.

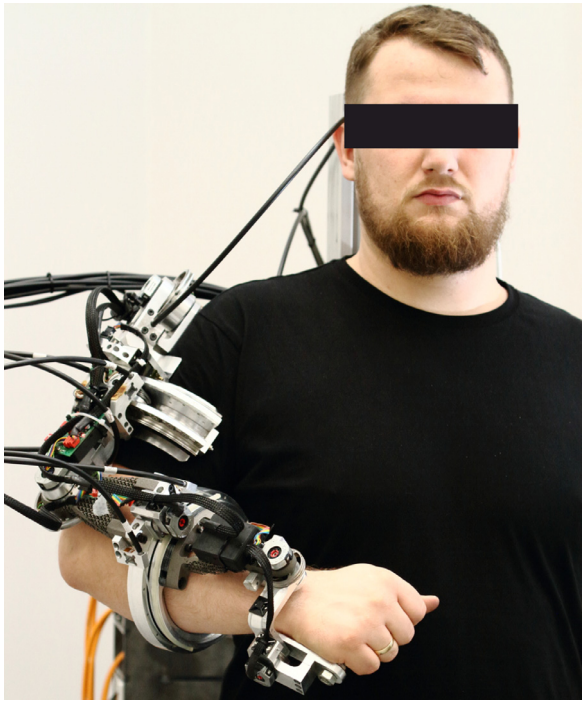

Fig. 17. Operator during tests of the torque control system.

b) The implementation of human body loading with a determined value of the interaction torque.

Achieving the functionality at a) is implemented with a given value $\tau_{iset} = 0$. As a result of the control system, the exoskeleton joint follows the operator's joint movement. This mode is used to scan human motion without load. Loading a human body with a torque of interaction can be used during teleoperations, control of virtual objects, and rehabilitation exercises.

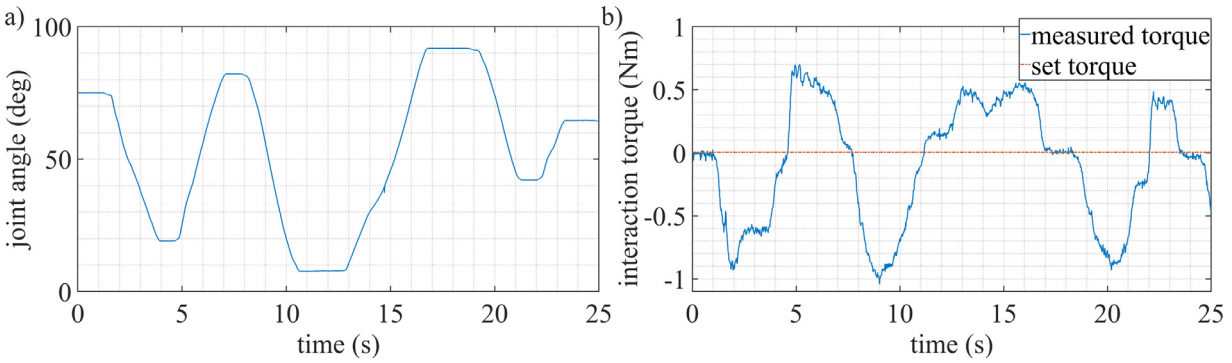

Fig. 18. a) Joint position during the test b) Measured and setpoint torque during the torque control system test at a setpoint value of 0 Nm.

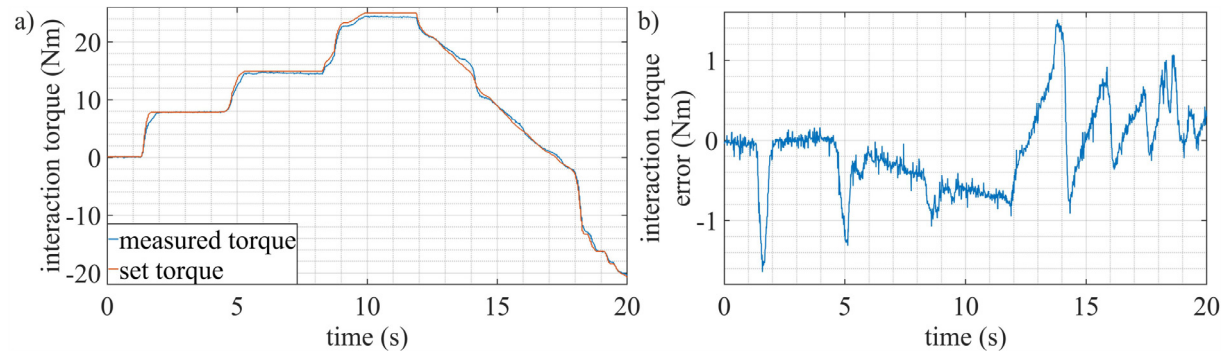

Fig. 19. a) Torque value during the test with blocked fourth joint b) Torque error during torque control method test with blocked fourth joint.

2. Results

An analysis of the applied drive structure cooperation with the control system during cooperation with the operator was performed. The examinations were carried out for all joints. However, the article presents the work of the joint's drive system with the most extensive range of angular motion. The article presents the course of driving torque during the operation of the fourth joint. Also, during the fourth joint operation, the largest failure of the interaction torque during control system operation was observed. During the first experiment, the torque interaction with a human was examined at the level of 0 Nm. Consequently, the device's load reduction mode was tested. The operator during the tests is presented in Fig. 17.

During the test, the operator should move his hand in the exoskeleton. The exoskeleton's movement followed the operator's arm movement (see Fig. 18a). It was observed that the interaction torque is not permanently maintained at 0 Nm. The interaction torque during the test movement had a maximum value of 1Nm (see Fig. 18b). In the fourth joint of the presented exoskeleton, this value corresponds to a load of about 3 N on the operator's hand.

In the subsequent experiment, the possibilities of generating force feedback by using a controlled system with a flexible mechanical structure were investigated. The joint was mechanically blocked in the selected position to generate stable interaction torque values generated by the ExoArm 7-DOF exoskeleton joint. The drive system is used to generate a specific torque value on the joint. There were rapid changes in the setpoint value during the experimental studies during 0–11 s and a slow change in the setpoint interaction torque during 11–20 s (see Fig. 19a). The control system is characterized by a rapid response to fast changes in the interaction torque reference value. The torque control error observed during the experiment was a maximum of −1.6 Nm (see Fig. 19b).

3. Conclusion

The device presented in this article is a mechatronic system compatible with the features of a wearable robot. The device replicates the kinematic structure of the human upper extremity resulting in a parallel kinematic chain. The device has seven active joints supplied with DC actuators through a pull-pull cable transmission system. The presented prototype of a wearable unit is also equipped with drive torque sensors integrated with pull-pull transmission elements. Furthermore, to increase the precision control of the interaction torque between the operator and the machine, a flexible component is introduced in the transmission path. The parameters of the flexible element were determined based on the joint's dynamic model and the data on human perception limitations. Adding flexibility into the transmission system results in a reduction in the oscillation generated during the joint's start-up. The article also presents a tested method of reducing the influence

of friction in the tendon system using the Stribeck effect compensator. The ExoArm 7-DOF exoskeleton dynamics model was used to determine the torque of interaction between the device's structure and the operator, which subtracts from the values of torque of forces applied on individual joints torque value resulting from the dynamics of motion of the device joints. Finally, the device and its control system were developed to enable cooperation with a human body with force feedback interaction. The control errors of the torque interaction between the setpoint and the implemented value are only 1.6 Nm in transition states. For future research, the device will be used as a master unit for teleoperating with a loading crane.

Declaration of Competing Interest

The authors declare that they have no known competing financial interests or personal relationships that could have appeared to influence the work reported in this paper.

Acknowledgments

The authors are grateful to the projects (No. PBS3/A6/28/2015) supported by the National Centre for Research and Development, Poland (NCBiR), under the Applied Research Programme.

References

[1] E. Ambrosini, et al., A myocontrolled neuroprosthesis integrated with a passive exoskeleton to support upper limb activities, J. Electromyogr. Kinesiol. 24 (Apr. (2)) (2014) Art. no. 2, doi:10.1016/j.jelekin.2014.01.006.
[2] J. Rosen, M. Brand, M.B. Fuchs, M. Arcan, A myosignal-based powered exoskeleton system, IEEE Trans. Syst., Man, Cybern. A 31 (May (3)) (2001) Art. no. 3, doi:10.1109/3468.925661.
[3] K. Anam, A.A. Al-Jumaily, Active exoskeleton control systems: state of the art, Proc. Eng. 41 (Jan.) (2012) 988–994, doi:10.1016/j.proeng.2012.07.273.
[4] G. Aguirre-Ollinger, J.E. Colgate, M.A. Peshkin, A. Goswami, Active-impedance control of a lower-limb assistive exoskeleton, in: 2007 IEEE 10th International Conference on Rehabilitation Robotics, Noordwijk, Netherlands, 2007, pp. 188–195, doi:10.1109/ICORR.2007.4428426. Jun..
[5] Z. Li, Z. Huang, W. He, C.-Y. Su, Adaptive impedance control for an upper limb robotic exoskeleton using biological signals, IEEE Trans. Ind. Electron. 64 (Feb. (2)) (2017) Art. no. 2, doi:10.1109/TIE.2016.2538741.
[6] K. Kiguchi, S. Kariya, K. Watanabe, K. Izumi, T. Fukuda, An exoskeletal robot for human elbow motion support-sensor fusion, adaptation, and control, IEEE Trans. Syst., Man, Cybern. B 31 (Jun. (3)) (2001) Art. no. 3, doi:10.1109/3477.931520.
[7] A.B. Zoss, H. Kazerooni, A. Chu, Biomechanical design of the Berkeley lower extremity exoskeleton (BLEEX), IEEE/ASME Trans. Mechatron. 11 (Apr. (2)) (2006) Art. no. 2, doi:10.1109/TMECH.2006.871087.
[8] Y. Shen, P.W. Ferguson, J. Rosen, Chapter 1 - upper limb exoskeleton systems—overview, in: J. Rosen, P.W. Ferguson (Eds.), Wearable Robotics, Academic Press, 2020, pp. 1–22.
[9] Y. Ren, H. Park, L. Zhang, Developing a whole-arm exoskeleton robot with hand opening and closing mechanism for upper limb stroke rehabilitation, in: 2009 IEEE International Conference on Rehabilitation Robotics, 2009, pp. 761–765, doi:10.1109/ICORR.2009.5209482. Jun..
[10] K. Yamamoto, M. Ishii, K. Hyodo, T. Yoshimitsu, T. Matsuo, Development of power assisting suit, JSME Int. J. Ser. C Mech. Syst. Mach. Elem. Manufac. 46 (3) (2003) Art. no. 3, doi:10.1299/jsmec.46.923.
[11] X. Gu, Y. Zhang, W. Sun, Y. Bian, D. Zhou, P.O. Kristensson, Dexmo: an inexpensive and lightweight mechanical exoskeleton for motion capture and force feedback in VR, in: Proceedings of the 2016 CHI Conference on Human Factors in Computing Systems, San Jose California USA, 2016, pp. 1991–1995, doi:10.1145/2858036.2858487. May.
[12] M.P. de Looze, T. Bosch, F. Krause, K.S. Stadler, L.W. O'Sullivan, Exoskeletons for industrial application and their potential effects on physical work load, Ergonomics 59 (May (5)) (2016) Art. no. 5, doi:10.1080/00140139.2015.1081988.
[13] P. Letier, E. Motard, J. Verschueren, EXOSTATION : haptic exoskeleton based control station, in: 2010 IEEE International Conference on Robotics and Automation, 2010, pp. 1840–1845, doi:10.1109/ROBOT.2010.5509423. May.
[14] H. Kazerooni, R. Steger, L. Huang, Hybrid control of the berkeley lower extremity exoskeleton (BLEEX), Int. J. Rob. Res. 25 (May (5–6)) (2006) Art. no. 5–6, doi:10.1177/0278364906065505.
[15] J. Li, R. Zheng, Y. Zhang, J. Yao, iHandRehab: an interactive hand exoskeleton for active and passive rehabilitation, in: 2011 IEEE International Conference on Rehabilitation Robotics, 2011, pp. 1–6, doi:10.1109/ICORR.2011.5975387. Jun..
[16] R.A.R.C. Gopura, K. Kiguchi, Mechanical designs of active upper-limb exoskeleton robots: state-of-the-art and design difficulties, in: 2009 IEEE International Conference on Rehabilitation Robotics, 2009, pp. 178–187, doi:10.1109/ICORR.2009.5209630. Jun..
[17] H. Kawamoto, Suwoong Lee, S. Kanbe, Y. Sankai, Power assist method for HAL-3 using EMG-based feedback controller, in: SMC'03 Conference Proceedings. 2003 IEEE International Conference on Systems, Man and Cybernetics. Conference Theme - System Security and Assurance (Cat. No.03CH37483), 2, Washington, DC, USA, 2003, pp. 1648–1653, doi:10.1109/ICSMC.2003.1244649.
[18] R.A.R.C. Gopura, K. Kiguchi, Y. Li, SUEFUL-7: a 7DOF upper-limb exoskeleton robot with muscle-model-oriented EMG-based control, in: 2009 IEEE/RSJ International Conference on Intelligent Robots and Systems, 2009, pp. 1126–1131, doi:10.1109/IROS.2009.5353935. Oct..
[19] T. Bosch, J. van Eck, K. Knitel, M. de Looze, The effects of a passive exoskeleton on muscle activity, discomfort and endurance time in forward bending work, Appl. Ergon. 54 (May) (2016) 212–217, doi:10.1016/j.apergo.2015.12.003.
[20] A. Nikkhah, C. Bradley, A. Sharif Ahmadian, Design, dynamic modeling, control and implementation of hydraulic artificial muscles in an antagonistic pair configuration, Mech. Mach. Theory 153 (Nov.) (2020) 104007, doi:10.1016/j.mechmachtheory.2020.104007.
[21] M. Shafiei, S. Behzadipour, Adding backlash to the connection elements can improve the performance of a robotic exoskeleton, Mech. Mach. Theory 152 (Oct.) (2020) 103937, doi:10.1016/j.mechmachtheory.2020.103937.
[22] Y. Shen, J. Rosen, Chapter 5 - EXO-UL upper limb robotic exoskeleton system series: from 1 DOF single-arm to (7+1) DOFs dual-arm, in: J. Rosen, P.W. Ferguson (Eds.), Wearable Robotics, Academic Press, 2020, pp. 91–103.
[23] A. Ammar, A. Bourek, A. Benakcha, Sensorless SVM-direct torque control for induction motor drive using sliding mode observers, J. Control Autom. Electr. Syst. 28 (Apr. (2)) (2017) 189–202, doi:10.1007/s40313-016-0294-7.
[24] D. Reigosa, Y. g Kang, M. Martínez, D. Fernández, J.M. Guerrero, F. Briz, SPMSMs sensorless torque estimation using high-frequency signal injection, IEEE Trans. Ind. Appl. 56 (May (3)) (2020) 2700–2708, doi:10.1109/TIA.2020.2975757.
[25] U.A.T. Hofmann, T. Bützer, O. Lambercy, R. Gassert, Design and evaluation of a Bowden-cable-based remote actuation system for wearable robotics, IEEE Rob. Autom. Lett. 3 (Jul. (3)) (2018) 2101–2108, doi:10.1109/LRA.2018.2809625.
[26] Q. Zhang, D. Sun, W. Qian, X. Xiao, Z. Guo, Modeling and control of a cable-driven rotary series elastic actuator for an upper limb rehabilitation robot, Front. Neurorobot. 14 (Feb.) (2020) 13, doi:10.3389/fnbot.2020.00013.

[27] Y.M. Senturk, V. Patoglu, MRI-VisAct: a Bowden-cable-driven MRI-compatible series viscoelastic actuator, Trans. Inst. Meas. Control 40 (May (8)) (2018) 2440–2453, doi:10.1177/0142331217730429.
[28] H. Park, Yupeng Ren, Li-Qun Zhang, IntelliArm: an exoskeleton for diagnosis and treatment of patients with neurological impairments, in: 2008 2nd IEEE RAS EMBS International Conference on Biomedical Robotics and Biomechatronics, 2008, pp. 109–114, doi:10.1109/BIOROB.2008.4762876. Oct..
[29] Y. Shen, J. Ma, B. Dobkin, J. Rosen, Asymmetric dual arm approach for post stroke recovery of motor functions utilizing the EXO-UL8 exoskeleton system: a pilot study, in: 2018 40th Annual International Conference of the IEEE Engineering in Medicine and Biology Society (EMBC), 2018, pp. 1701–1707, doi:10.1109/EMBC.2018.8512665. Jul..
[30] P. Herbin, Design and modeling of an exoskeleton torque sensor, Zeszyty Naukowe Akademii Morskiej w Szczecinie 51 (123) (2017) vol. nrAccessed: Sep. 09, 2020. [Online]. Available: http://yadda.icm.edu.pl/baztech/element/bwmeta1.element.baztech-09ce068d-2a7a-4203-b98a-3e40bae5582a .
[31] U. Jeong, K. Cho, Feedforward friction compensation of Bowden-cable transmission via loop routing, in: 2015 IEEE/RSJ International Conference on Intelligent Robots and Systems (IROS), 2015, pp. 5948–5953, doi:10.1109/IROS.2015.7354223. Sep..
[32] U. Jeong, K.-J. Cho, Control of a Bowden-Cable actuation system with embedded BoASensor for soft wearable robots, IEEE Trans. Ind. Electron. 67 (Sep. (9)) (2020) 7669–7680, doi:10.1109/TIE.2019.2945212.
[33] B.K. Dinh, L. Cappello, M. Xiloyannis, L. Masia, Position control using adaptive backlash compensation for bowden cable transmission in soft wearable exoskeleton, in: 2016 IEEE/RSJ International Conference on Intelligent Robots and Systems (IROS), Daejeon, South Korea, Oct. 2016, pp. 5670–5676, doi:10.1109/IROS.2016.7759834.
[34] S. Hirche, M. Buss, Human-oriented control for haptic teleoperation, Proceed. IEEE 100 (Mar. (3)) (2012) 623–647, doi:10.1109/JPROC.2011.2175150.
[35] P. Herbin, M. Pajor, ExoArm 7-DOF (interactive 7-DOF Motion controller of the operator arm) master device for control of loading crane, in: A. Hamrol, O. Ciszak, S. Legutko, M. Jurczyk (Eds.), Advances in Manufacturing, Springer International Publishing, Cham, 2018, pp. 439–449.
[36] P. Herbin, M. Pajor, Interactive 7-DOF motion controller of the operator arm (ExoArm 7-DOF), in: 2017 IEEE International Conference on INnovations in Intelligent SysTems and Applications (INISTA), Gdynia, 2017, pp. 185–188, doi:10.1109/INISTA.2017.8001154. Jul..
[37] M. Saków, K. Marchelek, Design and optimisation of regression-type small phase shift FIR filters and FIR-based differentiators with optimal local response in LS-sense, Mech. Syst. Signal Process (Nov.) (2020) 107408, doi:10.1016/j.ymssp.2020.107408.
[38] Kok Kiong Tan, T.H. Lee, S.N. Huang, Xi Jiang, Friction modeling and adaptive compensation using a relay feedback approach, IEEE Trans. Ind. Electron. 48 (Feb. (1)) (2001) 169–176, doi:10.1109/41.904577.
[39] L. Marton, B. Lantos, Modeling, identification, and compensation of stick-slip friction, IEEE Trans. Ind. Electron. 54 (Feb. (1)) (2007) 511–521, doi:10.1109/TIE.2006.888804.
[40] L. Márton, B. Lantos, Control of mechanical systems with Stribeck friction and backlash, Syst. Control Lett. 58 (Feb. (2)) (2009) 141–147, doi:10.1016/j.sysconle.2008.10.001.